Progress In Electromagnetics Research M, Vol. 103, 61–70, 2021

Statistical Channel Models for Millimeter-Wave Wireless Data Centers

Mohammed Z. Zaaimia[1, *], Rachida Touhami[2], Larbi Talbi[3], Mourad Nedil[4], and Mustapha C. E. Yagoub[5]

Abstract—This paper presents a set of statistical channel models based on 60 GHz radio measurements in a server room. The channel models are developed for possible use-cases, corresponding to potential deployment scenarios in wireless data centers (WDCs). A simple parametric channel model is used to model both the deterministic and stochastic channel parameters in the delay domain, within the 57–64 GHz unlicensed band. A simulation framework is accordingly provided to generate channel realizations for WDC use cases. The accuracy of the simulation framework is verified using the delay spread as a validation metric. The reported models are useful for practical system design and evaluation of WDCs millimeter-wave systems.

1. INTRODUCTION

The demand for new technologies capable of delivering high throughput in data centers (DC) is higher than ever before. The introduction of multi-gigabit wireless links in data centers has received considerable interest in recent years [1–5]. Wireless data centers (WDC) can potentially augment or replace the wired data center network (DCN) using optical or radio links. 60 GHz wireless links can alleviate over-subscription by providing flexible and instantaneous extra-bandwidth using direct line-of-sight (LoS) between top-of-racks (ToRs). Wireless links can also offer efficient network switching using beamsteering, resulting in reduced costs and low latency [6]. As such, WDC links can potentially increase the reliability, fault tolerance, and failure resiliency. WDCs are foreseen as an emerging use-case in the IEEE 802.11ay 60 GHz standard [7, 8]. The IEEE 802.11ay devices can achieve up to a 100 Gb/s data rate [9]. Thus, 60 GHz WDC links can potentially match the wired DCN in terms of performance, without the downsides of logistics and cost challenges.

Transmission mechanisms and system design at 60 GHz are strongly dependent on the propagation environment, due to the small wavelength ($\lambda = 5$ mm) [10]. 60 GHz radio links are heavily attenuated, and signals are distorted by reflected and scattered multipath components (MPCs) [11]. 60 GHz WDC propagation channel is characterized by rich reflections from ToRs and surrounding objects, due to the abundance of metallic scatterers in DC environments. In fact, in our previous work [12, 13], we observed double bounce reflections from the surrounding metallic objects and up to the fourth order reflections in [4]. As such, the WDC radio channel can significantly vary depending on the WDC deployment scenario and cannot be modeled only by a single slope channel response. Therefore, use-case specific channel modeling is crucial for WDC system design and evaluation.

Received 25 April 2021, Accepted 24 June 2021, Scheduled 27 June 2021
* Corresponding author: Mohammed Zakarya Zaaimia (m.zaaimia@univ-jijel.dz).
[1] Science and Technology Faculty, University of Jijel, Jijel 18000, Algeria. [2] Electronics and Computer Science Faculty of the University of Sciences and Technology Houari Boumediene, Algiers 16111, Algeria. [3] Department of Computer Science and Engineering of University of Quebec in Outaouais, Gatineau, QC J9A 1L8, Canada. [4] University of Quebec in Abitibi-Temiscamingue (UQAT), Val- d'Or, QC J9P 1S2, Canada. [5] School of Electrical Engineering and Computer Science, University of Ottawa, Ottawa, ON K1N 6N5, Canada.

This paper reports a statistical channel modeling effort based on 60 GHz radio measurements in a server room. Using a vector network analyzer (VNA) based channel sounder, the WDC channel characteristics are investigated to develop statistical channel models capable of reproducing and expressing the deterministic and stochastic channel parameters in the delay domain. WDC channel measurements and modeling are driven by the need for channel models to design reliable and densely connected WDCs. To the best of our knowledge, only racktop-to-racktop scenarios were investigated in a quasi-deterministic-map-based modeling effort in [4]. This approach is dependent on the environment geometry, and therefore, it provides an environment dependent channel parameters. In contrast, we report a generic channel modeling effort that considers the practical deployment scenarios in a WDC. The original contributions of this paper are twofold. *First*, we investigate the directional WDC propagation characteristics in the 57–64 GHz band for possible WDC deployment scenarios. *Second*, we propose a set of parametric statistical channel models along with a simulation framework to generate the channel response for potential WDC LoS use-cases.

2. CHANNEL MEASUREMENTS IN DATA CENTER ENVIRONMENT

The WDC measurement campaign was conducted in the campus server room of the University of Quebec in Outaouais, Gatineau, Canada. The characteristics of the server room are detailed in [12].

2.1. Measurement Scenarios

The three WDC use-cases investigated in this paper are cross-aisle-ToR (XToR), Neighbor-ToR (NToR) links, and server-to-server (S2S) use-case. XToR links are formed between two different ToRs from distinct rack rows separated by an aisle, whereas NToR links are established between neighboring contiguous racks. S2S links are established between servers within facing server-racks, as shown in [12]. The measured distances across use-cases were chosen considering the aforementioned deployment scenarios. As DC equipment is size and structure-standardized, the chosen distances correspond to the practical deployment scenarios in a real DC.

2.1.1. Cross-Aisle ToR

As shown in Figure 1(a), the XToR measurements were performed with the Rx antenna mounted on R5 $(60 \times 110 \times 200)\,\text{cm}^3$, with different ToR heights (relative to the ToR) and corresponding depths

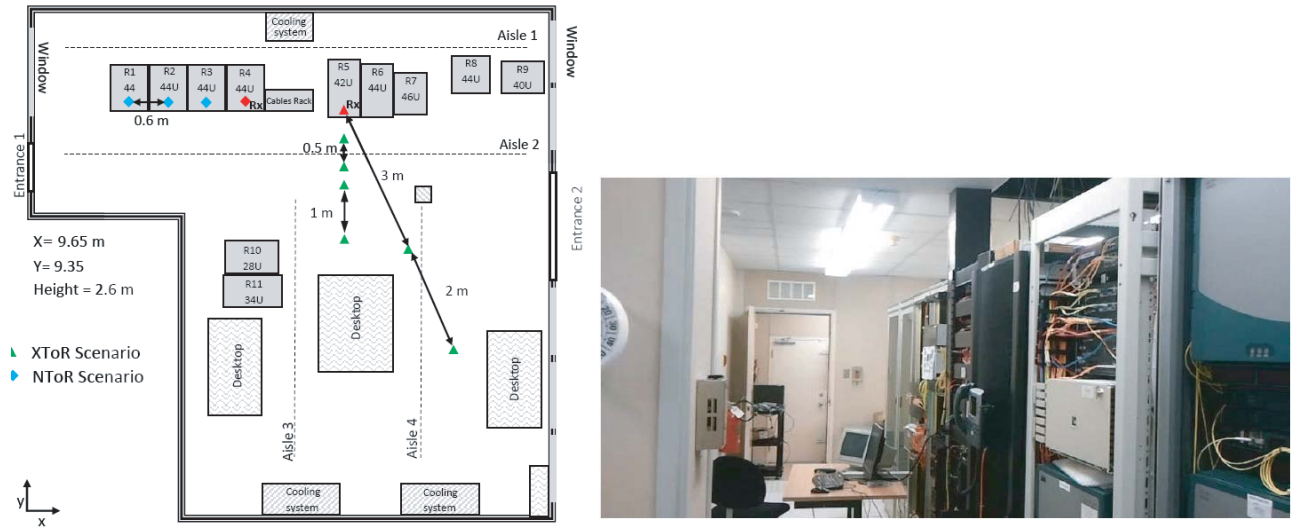

Figure 1. Campus server room layout: (a) Campus data center environment floor plan (not in scale) with measurement scenarios, and (b) photography of a rack-row.

Table 1. Measurement parameters.

WDC Use-case	Tx-Rx antennas	Antenna ToR depth (cm)	Antenna ToR height (cm)	Tx-Rx range (m)
XToR	Horn-Horn	20, 33	13, 15	0.5–5
NToR	Horn-Horn	20, 33	13, 15	0.6–1.8
S2S	Horn-Horn	-	-	0.2–1.6

(relative to the front of the rack), shown in Table 1. The Tx antenna was moved up to 5 m to cover practical aisle widths in DCs. The Tx antenna height was matched in optimal LoS with the Rx antenna at each ToR height, i.e., 13 cm and 15 cm. At each Tx-Rx measured location, 10 power delay profiles (PDPs) were measured per height/depth combination, i.e., (13 cm, 20 cm) and (15 cm, 33 cm). Each PDP is averaged from 10 snapshots to reduce random noise. The total number of measured PDPs at six locations is: $10 \times 10 \times 2 \times 6 = 1200$ PDPs (120 averaged PDPs).

2.1.2. Neighbor ToR

The Rx antenna was mounted on R4, and the Tx antenna was moved on R1 and R2 with similar height/depth combinations to XToR use-case. The channel response for directly adjacent ToRs was found deterministic, as the antennas' spatial filtering omits MPCs at small distances. As such, only distant-neighboring racks from R4 (i.e., R2 and R1) were considered. The corresponding measured distances are shown in Table 1. The total number of measured PDPs at two locations is: $10 \times 10 \times 2 \times 2 = 400$ PDPs (40 averaged PDPs).

2.1.3. Server-to-Server

To emulate two vertically facing servers in S2S configuration, the Tx and Rx antennas were mounted on two slotted steel bars at a 1 m height above the floor. The width of the metal bars is 4 cm, which is slightly smaller than a rack unit width $U = 4.445$ cm. The measurement distance was varied from 0.2 m up to 1.6 m to cover the intra-rack and inter-rack practical separations and quantify the specular reflections from the metallic bars. For each distance, a total of 20 averaged PDPs were measured in two different locations along Aisle-2, shown in Figure 1(b). The total number of measured PDPs for the eight locations is 1600 (160 averaged PDPs).

2.2. Measurements Setup and Data Processing

The used channel sounder is based on a VNA capable of stable measurement up to 70 GHz. The Tx and Rx sides are composed of a power amplifier (PA) and a low noise amplifier (LNA) at the Tx and Rx sides, respectively, with identical extension cables (amplitude and phase stable [14]) and identical horn antennas. The channel sounder setup and used settings are tabulated in Table 2. The horn antennas (with a 3 dB-beamwidth of 24°) were used in both sides with vertical polarization. The used antennas can operate in the 50–75 GHz band; therefore, the effect of cross-bandwidth gain variation was assumed flat in the measured band (around 0.4 dB in the 57–64 GHz band [15]). A back-to-back calibration was performed before the measurements and the delay from the nominal velocity in the cables accounted for. We stress that the antennas are not included in the calibration, thus, the antennas effects are implicitly considered as a part of the channel. Interested readers in the measurement setup refer to [16, 17].

At each measured location, the snapshots of the channel transfer function (CTF) were measured in the frequency domain. A data pool of all measurement scenarios was built and normalized to the transmit power. The discrete complex CTF is given by a complex exponential expression as:

$$H(f) = \left\{ A_n \cdot e^{(j\theta_n)} \right\} \tag{1}$$

where A_n and θ_n are the magnitude and phase of the measured S_{21}-parameter at a frequency point $1 \leqslant n \leqslant 7001$. The measured complex CTF is a vector of N_f measured points. The averaged PDP is

Table 2. Channel sounder settings and parameters.

Setup Parameters	Characteristics
VNA	Anritsu MS-4647A
PA gain (CERNEX CBM 57653/015-03)	30 dB
LNA gain (CERNEX CBL 57653/055-01)	30 dB
Tx Cable (Phase shift stable)	4.6 m (32 dB attenuation)
Rx Cable (Phase shift stable)	4.6 m (32 dB attenuation)
Tx, Rx Antenna gain (Millitech SGH-15)	23.3 dBi Horn-(V-V)
Bandwidth (BW)	7 GHz (57–64 GHz)
Dynamic range	$\sim$ 90 dB
Sweep points (N_f)	7001
Frequency step (Δf)	1 MHz
Delay resolution	142.85 ps

deduced from Eq. (1) by applying an inverse discrete Fourier transform on the CTF as:

$$PDP(\tau) = \frac{1}{S}\sum_{s=1}^{S} |\mathrm{IDFT}\{H(f)\cdot w\}|^2 \tag{2}$$

where s is the PDP snapshot $1 \leqslant s \leqslant 10$. w_n is a Kaiser windowing function (of size N_f) used to reduce side lobes.

The large-scale path loss was modeled in [12] by a log-distance model as:

$$PL(d) = PL(d_0) + 10\cdot n\log_{10}(\frac{d}{d_0}) + X_{\sigma_s} \tag{3}$$

where n is the path loss exponent, PL (d_0) i the path loss at a reference distance $d_0 = 1$ m, and X_{σ_s} the shadow fading.

3. WDC STATISTICAL CHANNEL MODELS

In this section, the channel models are developed to express the channel response for WDC use-cases.

3.1. Parametric Model

The shape of the measured PDPs is composed of a LoS component followed by a decaying clutter and specular components in the form of distinguishable peaks. The PDP for WDC use-cases can be expressed by a simple parametric model as:

$$PDP(\tau)=\begin{cases} P_{LoS}, & \tau = \tau_0 \\ \sum_{n=1}^{N_s} P_{sc}.\delta(\tau-\tau_n) + P_{df}.e^{\frac{-(\tau-\tau_0)}{\beta}}, & \tau_0 < \tau \leqslant \tau_c \end{cases} \tag{4}$$

where N_s is the number of enumerated specular components. τ_0 is the time of arrival (ToA) of the LoS component, and τ_c is the maximum excess delay. P_{sc} and τ_n are the power and the excess delay of the nth specular component. P_{df} is the onset power of the diffuse component, and β is the exponential decay constant. As the LoS components' ToA is modeled deterministically, the PDPs are delay-normalized with respect to the LoS time-of-arrival τ_0, i.e., $\tau_0 = 0$. Therefore the delay of the PDP components after the LoS component is considered as an absolute excess delay.

3.2. Statistical Processing

The specular components powers, P_{sc}, and their corresponding excess delays are extracted using a peak detection method. The method operates as:

(i) *Identify* the first most significant peak and *get* its ToA in the delay domain.

(ii) *Identify* all peaks above a 30 dB threshold with respect to the peak identified in step 1.

(iii) *If* $peak_n < peak_{n-1}$, and a 6 dB minimum below $peak_n$ (in the delay interval between $peak_n$ and $peak_{n-1}$) is found, *then* identify $peak_n$ as the beginning of a cluster of specular components.

The 6 dB threshold here is a heuristic value that can efficiently enumerate up to 95% of the specular components. The diffuse components statistics were extracted from the onset power of the local power minimum after the LoS components. Moreover, the delay between specular components, denoted as ξ, is extracted accordingly from the ToA of the detected specular components. ξ statistical distribution is used to model the specular components' arrival rate. The model parameters P_{sc}, P_{df}, and β are modeled by a linear least-square regression, as shown in Figure 2, Figure 3, and Figure 4, whereas the excess delay between specular components, ξ, is modeled statistically.

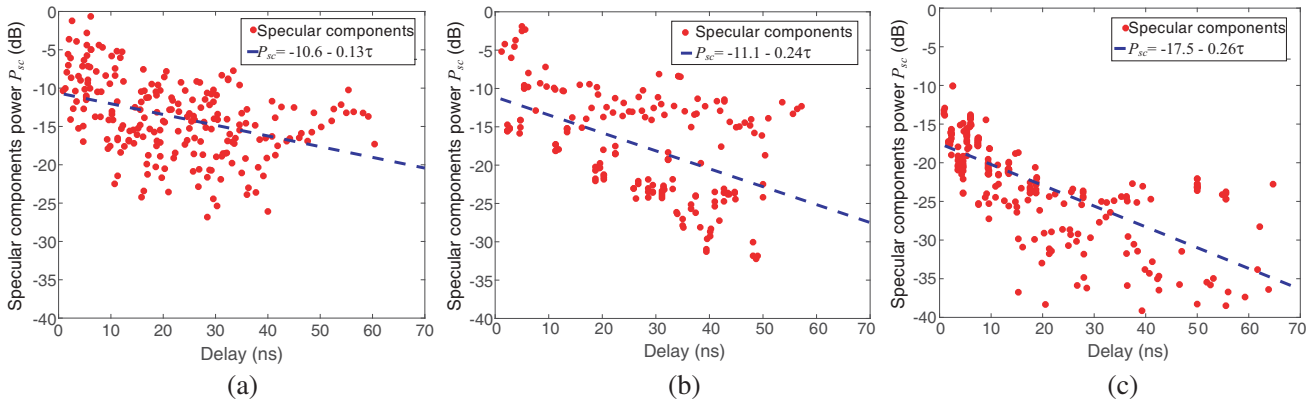

Figure 2. The normalized power of the specular components P_{sc}, relative to P_{LoS}: (a) XToR, (b) NToR, and (c) S2S.

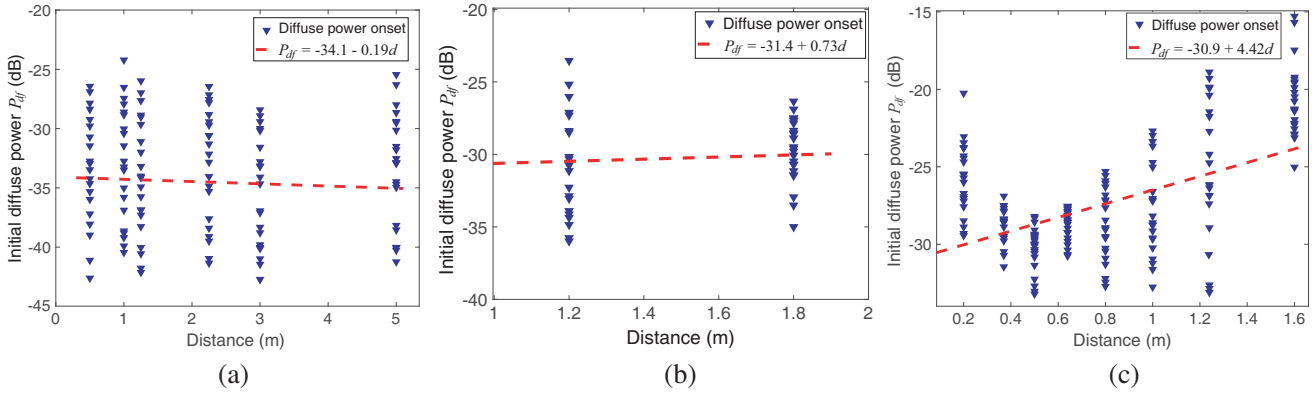

Figure 3. The diffuse power P_{df}, relative to P_{LoS}: (a) XToR, (b) NToR, and (c) S2S.

The specular components power, P_{sc}, is dependent on the excess delay, as shown in Figure 2. The linear regression expressions for the XToR, NToR, and S2S use-cases are tabulated in Table 3. P_{sc} statistical deviations were best fitted with a Gamma distribution ($\Gamma(\mu, \sigma)$ in linear scale) for the XToR and S2S use-cases, and a lognormal distribution ($\mathrm{L}(\mu, \sigma)$) for the NToR use-case. The delay between

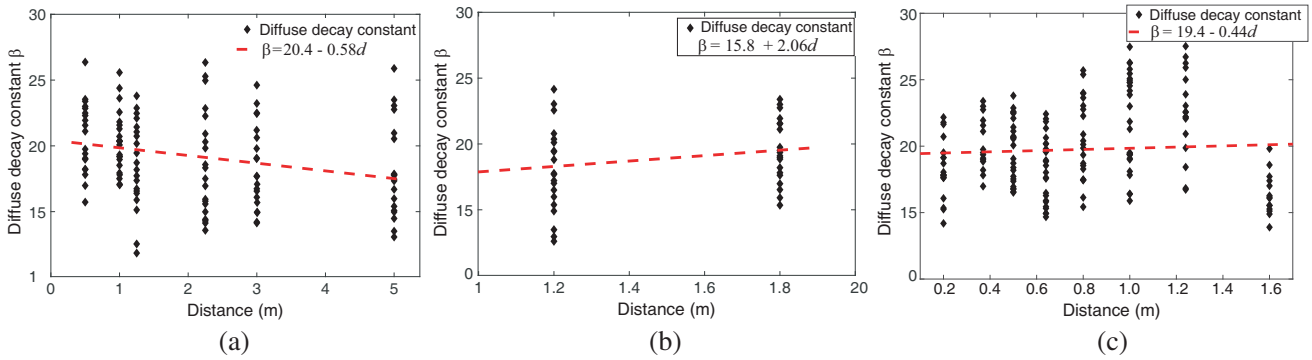

Figure 4. The decay constant β: (a) XToR, (b) NToR, and (c) S2S.

Table 3. Wireless data center channel model parameter.

		XToR		NToR		S2S	
Parameters	Unit	Linear fit	Deviation (μ, σ)	Linear fit	Deviation (μ, σ)	Linear fit	Deviation (μ, σ)
P_{sc}	dB	$-10.6 - 0.13\tau$	Γ $(a = 3.91,$ $b = 0.28)$	$-11.1 - 0.24\tau$	$L(0.01, 0.68)$	$-17.5 - 0.26\tau$	Γ $(a = 3.97,$ $b = 0.28)$
P_{df}	dB	$-34.1 - 0.19d$	Γ $(a = 2.61,$ $b = 0.46)$	$-31.4 + 0.73d$	$L(0, 0.40)$	$-30.9 + 4.42d$	$L(0.01, 0.36)$
β	-	$20.4 - 0.58d$	$\mathcal{N}(0.05,\ 3.22)$	$15.8 + 2.06d$	$\mathcal{N}(0.08,\ 3.62)$	$19.4 + 0.44d$	$\mathcal{N}(0.08,\ 3.17)$
ξ	ns	-	$L(0.04, 0.67)$	-	$L(0.42, 0.68)$	-	$L(0.55, 0.84)$
PL (d_0) [12]	dB	76.63		76.00		67.08	
n [12]	-	2.02		1.77		1.11	
σ_s [12]	dB	$L(0, 2.81)$		$L(0, 1.63)$		$L(0, 2.74)$	
Rx-Tx distance	m	[0.5–5)		[1.2–1.8)		[0.2–1.6)	

specular components, ξ, was best fitted by a lognormal distribution across all use-cases, as shown in Figure 5. The linear fits of the initial diffuse component power, P_{df}, shown in Figure 3, are tabulated in Table 3. The deviations from the fitted lines were best fitted by a lognormal distribution for the NToR and S2S use-cases, and a Gamma distribution for the XToR use-case. Moreover, the linear fits of the decay constant, β, shown in Figure 4 are tabulated in Table 3. The deviations of the decay constant from the fitting lines were found normally distributed $(\mathcal{N}(\mu, \sigma))$.

Across all WDC use-cases, the shadowing statistical parameters were best fitted with a Gaussian, Gamma, or lognormal distributions. P_{df} and P_{sc} deviations were also found lognormally distributed in [18, 19]. In [18], β was modeled by its mean, as it shows no dependency on the measurement distance, whereas in our case, β shows a slight variation against distance in all WDC use-cases. The variations are partly attributed to the wider measurement bandwidth (cf. [18]) and measured distances. Moreover, the delay between specular components, ξ, was best-fitted by an exponential distribution in [4, 18, 19], compared to a lognormal distribution in our cases.

4. CHANNEL MODEL IMPLEMENTATION

4.1. Model Assumptions and Considerations

The developed WDC models are use-case specific, i.e., model results, behaviors, and inferred conclusions are specific to the deployment scenario's measured distance. As such, the models are valid only for LoS links within the investigated distances. Also, the channel models output is only valid for the measured

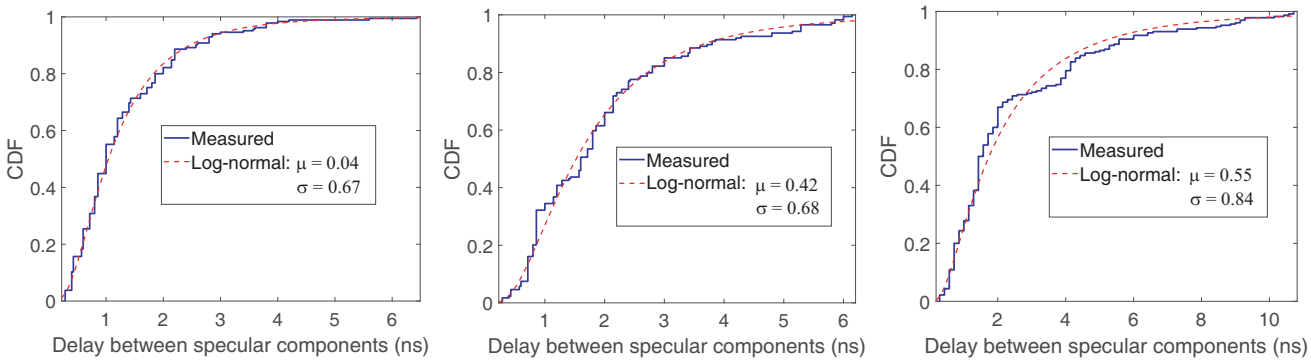

Figure 5. The cumulative distribution functions (CDFs) of the delay between specular components (ξ) and fitted CDF: (a) XToR, (b) NToR, and (c) S2S.

band (57–64 GHz), under quasi-static WSSUS (Wide-Sense Stationary Uncorrelated Scattering) channel assumption, as higher frequency bands have different characteristics [19]. As we used vertically polarized highly directive antennas in our measurements, the antennas directivity is implicitly embedded in the channel models; therefore, the models are valid for similar highly directive antennas (with vertical polarization), regardless of their gain, as the latter was omitted from the measurements in [12]. As such, we assert that one can add his own directive antenna gains in the channel model realizations and link budget calculations.

4.2. Implementation Steps

Depending on the WDC use-case, the channel model can be easily implemented to generate the PDP, channel impulse response (CIR), and CTF using the following steps:

(i) Define (user inputs):
  (a) The number of frequency points N_f.
  (b) Bandwidth BW.
  (c) Tx-Rx distance d (the channel model is valid only for the measured distances, illustrated in Table 3.
  (d) Set the theoretical maximum excess delay, τ_c, defined as: $\tau_c = 1/\Delta f$, where Δf is the frequency step, defined as: $\Delta f = BW/(N_f - 1)$. Note that the channel models are only valid for $\tau_c \leqslant 70$ ns.

(ii) Calculate the path loss using Eq. (3), with the shadowing parameters in Table 3.

(iii) Calculate the time of arrival of the LoS component, τ_0, using the Tx-Rx distance d as: $\tau_0 = d/c$, where c is the speed of light.

(iv) Generate the delay values between specular components, ξ, using the log-normal distribution parameters in Table 3. Add ξ values to τ_0 until the maximum excess delay (τ_c), defined in step (1.d), is reached.

(v) Calculate :
  (a) The specular components power, P_{sc}, using the corresponding fitting equation and add the corresponding shadowing in Table 3. Note that the parameters of the shadowing distributions are in linear scale, i.e., the generated shadowing values must be converted to dB scale. The Gamma probability distribution function is given as:

$$f(x|a,b) = \frac{1}{b^a \Gamma(a)} x^{a-1} e^{\frac{-x}{b}}$$

  where $\Gamma(\cdot)$ is the Gamma function, and a and b are the shape and scale parameters, respectively.

(b) The initial diffuse power value, P_{df}, using the equation in Table 3, and add the corresponding shadowing. Note that the parameters of the distributions are in linear scale.
(c) The decay constant, β, value using the equation in Table 3 and add the normally distributed deviation.

(vi) Generate the PDP using Eq. (4), with a $1/BW$ delay resolution and normalize the PDP to the path loss, calculated in step 2.

(vii) The CIR can be deduced as the square root of the generated PDP, whereas the frequency response can be calculated using a Fourier transform on the complex time domain response, after allocating random phase values between $[0, 2\pi]$ to the PDP components.

The output can be used as a tapped or clustered delay line in a block-fading-channel after normalization, that is $\int_0^{\tau_c} PDP(\tau)d\tau = 1$. An example of the channel model output is shown in Figure 6(b), for S2S use-case at a distance $d = 0.62$ m. Compared to the measured PDP in Figure 6(a), the simulated PDP shows reasonable similarities. The validation of the channel models accuracy is carried out in the next subsection.

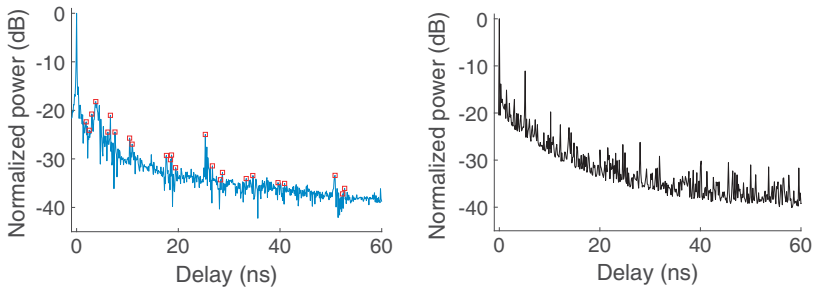

Figure 6. Power delay profiles for S2S use-case at $d = 0.62$ m: (a) measured PDP with the MPCs detection method output (in red squares), and (b) random realization of the S2S channel model.

4.3. Channel Models Validation

To validate the channel model consistency, we compare herein the root-mean-square delay spread (τ_{rms}) values of the measurements with those from the generated PDPs, for a given number of realizations. The channel model realizations are generated with the same measurement parameters and the same number of statistical samples, to avoid any statistical bias. As shown in Figure 7, the delay spread values from the channel models realizations seem slightly smaller at small distances than the measured values. The linear fitting shows an excellent match for the measured and simulated results in S2S and XToR cases, as confirmed by the CDF curves (Figure 8(a) and Figure 8(c)) and the mean, median, and

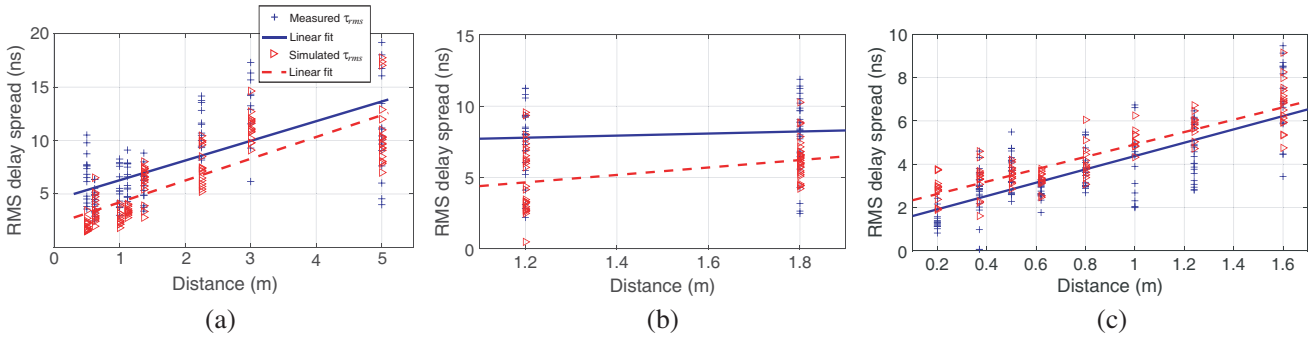

Figure 7. Measured and simulated RMS delay spread values: (a) XToR, (b) NToR, and (c) S2S.

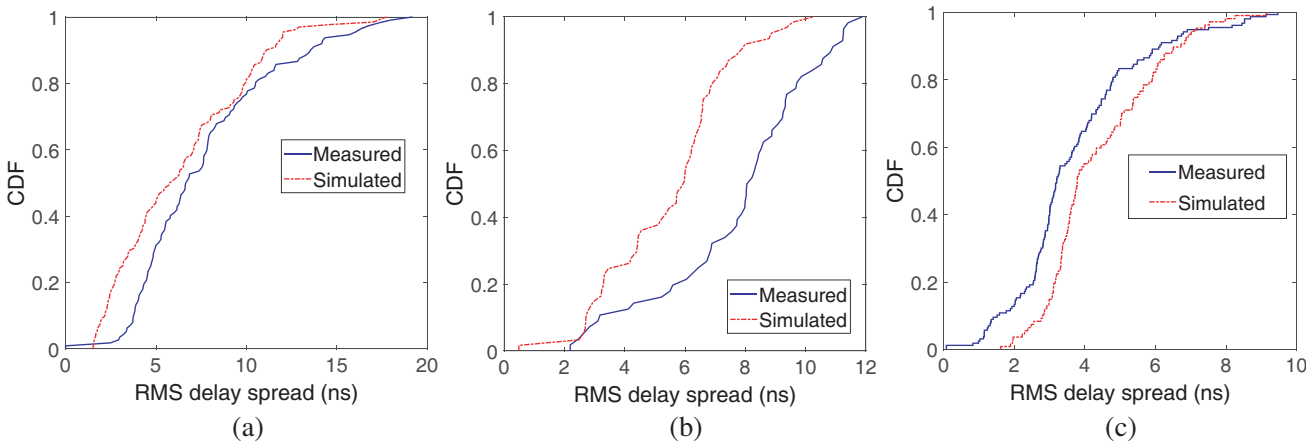

Figure 8. Cumulative distribution functions of the measured and simulated RMS delay spread: (a) XToR, (b) NToR, and (c) S2S.

standard deviations in Table 4. On the other hand, although NToR's delay spread values fall within the measurements range in Figure 7(b), the delay spread CDF in Figure 8(b) shows more variation than XToR and S2S cases. This slight variation can be attributed partly to the small number of measured positions and the dynamic evolution of propagation paths in each position. We do not consider this as a shortcoming of the NToR channel model, because the overall τ_{rms} statistics are within an acceptable range, as illustrated in Table 4.

Table 4. Measured and simulated RMS delay spread comparison.

	XToR			NToR			S2S		
τ_{rms}	μ	Mdn	σ	μ	Mdn	σ	μ	Mdn	σ
Measured [ns]	7.69	6.69	3.86	7.80	8.13	2.49	3.67	3.19	1.80
Simulated [ns]	6.39	5.84	3.71	5.53	5.98	2.03	4.36	3.78	1.55

5. CONCLUSION

In this paper, statistical channel models for WDC use-cases were developed to advance WDCs practical implementation from the channel modeling front. The channel model accuracy was validated using the delay spread as a validation metric. The simulated delay spread values fall within the measurements range, demonstrating that the channel models reflect the measured channel characteristics. The WDC channel modeling is motivated by the necessity of channel models to design and evaluate WDC 60 GHz multi-gigabit links. By exploiting the WDC channel models, accurate scheduling and channel allocation schemes can benefit from a comprehensive study of the channel capacity and achievable data rates in a WDC realistic channel. As DCs have predefined use-cases and fixed nodes, with pre-known spatial coordinates, WDC channel modeling is relatively universal and valid for a variety of DC structures and fabrics, since DC equipment (racks, cages,. . .) are size and structure-standardized.

REFERENCES

1. Hamza, A. S., J. S. Deogun, and D. R. Alexander, "Wireless communication in data centers: A survey," *IEEE Communications Surveys & Tutorials*, Vol. 18, No. 3, 1572–1595, 2016.
2. Cheng, C.-L., S. Sangodoyin, and A. Zajić, "Thz cluster-based modeling and propagation characterization in a data center environment," *IEEE Access*, Vol. 8, 56 544–56 558, 2020.

3. Cheng, C.-L. and A. Zajić, "Characterization of propagation phenomena relevant for 300 GHz wireless data center links," *IEEE Transactions on Antennas and Propagation*, 2019.
4. Gentile, C., P. B. Papazian, R. Sun, J. Senic, and J. Wang, "Quasi-deterministic channel model parameters for a data center at 60 GHz," *IEEE Antennas and Wireless Propagation Letters*, Vol. 17, No. 5, 808–812, 2018.
5. Celik, A., A. AlGhadhban, B. Shihada, and M. Alouini, "Design and provision of traffic grooming for optical wireless data center networks," *IEEE Transactions on Communications*, Vol. 67, No. 3, 2245–2259, 2019.
6. Katayama, Y., K. Takano, Y. Kohda, N. Ohba, and D. Nakano, "Wireless data center networking with steered-beam mmwave links," *2011 IEEE Wireless Communications and Networking Conference*, 2179–2184, IEEE, 2011.
7. TG11ay, "IEEE 802.11ay use cases. IEEE standard 802.11-2015/625," *Tech. Rep.*, IEEE, 2015.
8. Zhou, P., K. Cheng, X. Han, X. Fang, Y. Fang, R. He, Y. Long, and Y. Liu, "IEEE 802.11 ay-based mmWave WLANs: Design challenges and solutions," *IEEE Communications Surveys & Tutorials*, Vol. 20, No. 3, 1654–1681, 2018.
9. Ghasempour, Y., C. R. da Silva, C. Cordeiro, and E. W. Knightly, "IEEE 802.11 ay: Next-generation 60 GHz communication for 100 Gb/s Wi-Fi," *IEEE Communications Magazine*, Vol. 55, No. 12, 186–192, 2017.
10. Siamarou, A. G., P. Theofilakos, and A. G. Kanatas, "60 GHz wireless links for HDTV: Channel characterization and error performance evaluation," *Progress In Electromagnetics Research*, Vol. 36, 195–205, 2013.
11. Shrivastava, P. and T. Rama Rao, "Performance investigations with antipodal linear tapered slot antenna on 60 GHz radio link in a narrow hallway environment," *Progress In Electromagnetics Research*, Vol. 58, 69–77, 2015.
12. Zaaimia, M., R. Touhami, L. Talbi, M. Nedil, and M. Yagoub, "60-GHz statistical channel characterization for wireless data centers," *IEEE Antennas and Wireless Propagation Letters*, Vol. 15, 976–979, 2015.
13. Zaaimia, M., R. Touhami, V. Fono, L. Talbi, and M. Nedil, "60 GHz wireless data center channel measurements: Initial results," *2014 IEEE International Conference on Ultra-WideBand (ICUWB)*, 57–61, IEEE, 2014.
14. MegaPhase, "Megaphase v band test cable," MegaPhase, Tech. Rep. [Online]. Available: www.megaphase.com/wp-content/uploads/2017/01/MegaPhase-V-Band-Test-Cable.pdf.
15. Millitech, "Standard Gain Horn (SGH) 15," smithsinterconnect, Tech. Rep. [Online]. Available: www.smithsinterconnect.com/products/defence-antenna-systems/ antenna-quasioptical-products/standard-gain-horn-(sgh)/.
16. Tariq, S. A. M., C. L. Despins, S. Affes, and C. Nerguizian, "Angular dispersion of a scattered underground wireless channel at 60 GHz," *IEEE Access*, Vol. 8, 67 572–67 580, 2020.
17. Ghaddar, M., I. B. Mabrouk, M. Nedil, K. Hettak, and L. Talbi, "Deterministic modeling of 5g millimeter-wave communication in an underground mine tunnel," *IEEE Access*, Vol. 7, 116 519–116 528, 2019.
18. Kyro, M., K. Haneda, J. Simola, K.-I. Takizawa, H. Hagiwara, and P. Vainikainen, "Statistical channel models for 60 GHz radio propagation in hospital environments," *IEEE Transactions on Antennas and Propagation*, Vol. 60, No. 3, 1569–1577, 2011.
19. Haneda, K., J. Järveläinen, A. Karttunen, M. Kyrö, and J. Putkonen, "A statistical spatio-temporal radio channel model for large indoor environments at 60 and 70 GHz," *IEEE Transactions on Antennas and Propagation*, Vol. 63, No. 6, 2694–2704, 2015.